Astronomy Reports, Vol. 44, No. 9, 2000, pp. 579–591. Translated from Astronomicheskiĭ Zhurnal, Vol. 77, No. 9, 2000, pp. 654–668.

Photometric Properties of Bars in Galaxies

A. S. Gusev

Sternberg Astronomical Institute, Universitetskiĭ pr. 13, Moscow, 119899 Russia
Institute of Solid-State Physics, Russian Academy of Sciences, Chernogolovka, Moscow oblast, 142432 Russia
Received September 6, 1999

Abstract—We have used surface photometry data for 100 barred galaxies to determine the *UBVRIJHK* surface brightnesses and color indices for the bars. Two peaks are observed in the distribution of the average bar *B* brightnesses: at 21.0^m/arcsec^2 and 22.2^m/arcsec^2, characteristic of late- and early-type galaxies, respectively. The average surface-brightness difference between the bar and the galaxy (within the 25.0^m/arcsec^2 isophote) increases from 1.1^m/arcsec^2 for SB0 galaxies to 2.3^m/arcsec^2 for SBc–IBm galaxies. In $(U-B)_0$–$(B-V)_0$, $(B-V)_0$–$(V-R)_0$, and $(B-V)_0$–$(V-I)_0$ two-color diagrams, for all morphological types, the bars are shifted leftward from normal color sequence for galaxies. This deviation is more pronounced for the outer than for the inner regions of the bars. Using evolutionary models, we show that this deviation is due to the scarcity of intermediate-age [$(1–9)\times10^9$ yrs] stars in bars. Possible origins for this anomalous composition of the stellar population are discussed. © *2000 MAIK "Nauka/Interperiodica"*.

1. INTRODUCTION

A statistical study of the photometric properties of galactic bars was initiated by Kalloglian [1], who determined the average surface brightnesses for nine galaxies and found the bar surface brightnesses to be roughly the same as for most galaxies: 20.90 ± 0.2^m/arcsec^2 in the *B* band. In the same study, he showed that about 75% of the bars had similar brightnesses, whereas the bar surface brightnesses in the remaining 25% of the galaxies were approximately 1^m fainter.

Elmegreen and Elmegreen [2] divided bars into two types, depending on the morphological type of their parent galaxy. The bars in early-type spirals (SB0–SBb) have flat brightness profiles along their major axes and are longer than the bars in late-type galaxies. In bars with flat photometric profiles, there is a continuous increase in the ellipticity of the isophotes along the bar [3]. The bars in late-type galaxies (SBc–IBm) are characterized by an exponential brightness decrease along their major axes. The ellipticity of the isophotes in such bars does not vary with distance from the center.

In contrast to bars with exponential brightness decreases, those with flat photometric profiles contain a relatively small amount of gas. This is evidently due to the fact that the gas content in early-type galaxies is, on average, lower than in late-type galaxies. OB associations are not uncommon at the ends of bars [4, 5]. Dust lanes along the leading edges of bars are also observed [6]. The bars in early-type galaxies are, on average, redder than those in late-type galaxies [7]. This is probably due to the fact that, on the whole, early-type galaxies are redder than late-type galaxies, due to the small contribution of the young stellar population to the total luminosity.

On the basis of photometric data, it was shown in [8] that there is no appreciable star formation in the bars of SBb galaxies, in contrast to SBc galaxies, in which there can be fairly intense star formation. Similar conclusions can be drawn from the study of Pronik [9], who considered the locations of bars of SBc galaxies in the two-color diagram.

Elmegreen *et al.* [10] explain the flat profiles of bars in early-type galaxies as a consequence of an excess of stars of all ages (both old and young) at the bar ends. Based on the *UBVR* colors of the SBbc galaxy NGC 151, whose bar has an exponential brightness decrease, it was concluded that intermediate-age stars are scarce in this bar [11].

The differences in the shapes of bars in early- and late-type galaxies could reflect the action of different mechanisms for bar formation in galaxies of different morphological types. It is generally believed that, in galaxies with rapidly rotating disks (when the disk rotation rate is much higher than the radial dispersion of the stellar velocities), bars are formed due to instability of the dynamically cold disk. The bars in such galaxies extend to the corotation region, since, at distances larger than the corotation radius, the main stable orbits become perpendicular to the major axis of the bar [12, 13]. The Lynden-Bell mechanism acts in galaxies with slowly rotating disks [14, 15]. Essentially, when stars are located in adjacent extended orbits, their orbits precess and approach each other due to gravitational instability, forming a bar. In this case, the radius of the bar cannot exceed the radius of the inner Lindblad resonance.

2. THE SAMPLE OF GALAXIES

Surface photometry has been performed for a large number of barred galaxies; however, these data have not been systematized. After surveying data published

Table 1. Average surface brightness and color indices of bars

	SB0 galaxies	*N*	SB0/Ba–SBbc galaxies	*N*	SBc–Ibm galaxies	*N*	All galaxies	*N*
$\langle B_0 \rangle$	22.04 ± 0.52	13	21.57 ± 0.56	32	20.93 ± 0.35	20		
$\langle V_0 \rangle$	21.36 ± 0.28	8	20.62 ± 0.38	24	20.47 ± 0.47	17		
$\langle (U-B)_0 \rangle$			0.13 ± 0.23	5	0.11 ± 0.27	10	0.12 ± 0.24	15
$\langle (B-V)_0 \rangle$	0.83 ± 0.18	8	0.82 ± 0.14	24	0.60 ± 0.23	16		
$\langle (V-R)_0 \rangle$	0.43 ± 0.08	6	0.43 ± 0.14	14	0.33 ± 0.12	9	0.40 ± 0.13	27
$\langle (R-I)_0 \rangle$	0.62 ± 0.15	7	0.70 ± 0.13	12	0.43 ± 0.06	3		
$\langle (I-J)_0 \rangle$							0.83 ± 0.16	3
$\langle (J-H)_0 \rangle$							0.66 ± 0.14	8
$\langle (H-K)_0 \rangle$							0.30 ± 0.07	6

over the last 40 years, we collected *UBVRIJHK* data for 100 barred galaxies. We sometimes used the average measured bar surface brightnesses directly. In most cases, however, we had to derive the average surface brightnesses and color indices from photometric profiles along the major axes of the bars. For "flat" bars, we used the brightness or color index averaged over the bar, while, for "exponential" bars, we used the values at half the length of the bar semimajor axis. In several cases, we used published isophote maps. The data were then corrected for Galactic absorption and absorption due to the inclination of the disk, in accordance with the technique proposed in the RC3 [16]. All the data were reduced to the Johnson–Cousins *UBVRI* and Elias *JHK* systems [17].

The resulting estimates of the surface brightnesses and color indices are summarized in an electronic table, which can be found in the Strasbourg CDS database and at the Internet site *http://lnfml.sai.msu.ru/~gusev/catalog/readme.html.* The columns of the table present (1) the NGC or IC numbers of the galaxies, (2) the morphological type of the galaxies according to the RC3, (3) the average surface brightnesses corrected for Galactic absorption and absorption due to the disk inclination in one of two indicated filters, (4)–(10) the bar color indices, and (11) the accuracy of the average bar surface brightnesses and color indices (the errors of the average values are presented). References to the initial sources are also given.

3. ANALYSIS OF THE PHOTOMETRIC DATA

3.1. Average Bar Surface Brightnesses

We divided all the galaxies into three groups according to morphological type: the first group includes 14 SB0 galaxies; the second, 47 SB0/Ba–SBbc galaxies; and the third, 39 SBc–IBm galaxies. For each of the three groups, we calculated the bars' average B_0 and V_0 surface brightnesses and the $(U-B)_0$, $(B-V)_0$, $(V-R)_0$, $(R-I)_0$, $(I-J)_0$, $(J-H)_0$, and $(H-K)_0$ color indices. These data are presented in Table 1, which also indicates the number of galaxies considered. We can see a pronounced correlation between the galaxy type and the average bar surface brightness: on average, the bars in late-type galaxies are brighter.

Figure 1 presents histograms of the average *B* surface-brightness distributions for the bars and their parent galaxies. The magnitudes corrected for absorption B_0^T, major axes D_0, and axis ratios R_{25} used to derive the values in the histogram in Fig. 1b were taken from the RC3. The two histograms differ considerably: the galaxy distribution is normal (Gaussian), with a maximum at 23.1^m/arcsec^2 and rms deviation 0.4^m/arcsec^2, while the bar distribution is bimodal and has a relatively large dispersion. A χ^2 test shows that the distribution in Fig. 1a is inconsistent with a normal distribution at the 0.91 significance level.

Two peaks can be seen in the brightness distribution for the bars (see the histogram in Fig. 1a): one at 21.0^m/arcsec^2 and a second, weaker, peak at 1.2^m/arcsec^2. This is in fairly good agreement with earlier studies (see, for example, [1]); however, there is no distinct division between these two maxima in our sample. The relative numbers of bright and weak bars (taking the boundary between them to be 21.67^m/arcsec^2, the local minimum in the histogram in Fig. 1a) also differ from those found earlier: 60 ± 10% bright bars and 40 ± 10% weak bars (as opposed to 75 and 25%, as found by Kalloglian [1]).

Note also the distribution for the second group of galaxies (SB0/Ba–SBbc): while the maximum for SB0 galaxies virtually coincides with the weak peak (in brightness) for the bars and the maximum for SBc–IBm galaxies coincides with the bright peak (Fig. 1a and Table 1), the distribution for SB0/Ba–SBbc galaxies is rather uniform over a wide range. These galaxies make up about half the galaxies contributing to both peaks (Fig. 1a), and their mean surface brightness (Table 1) lies between the two maxima in the histogram.

Thus, the bars can be divided into two photometric types according to parent galaxy type: early- and late-type

bars. SB0/Ba–SBbc galaxies possess bars of both types. This is in agreement with the results of Elmegreen and Elmegreen [2], who divided bars into two types according to their photometric profiles and relative lengths (see Section 1).

The difference between the average surface brightness of the bar and of the galaxy as a whole, $B_{0,\mathrm{bar}} - \mu(B_0)_{\mathrm{gal}}$, increases from 1.1 ± 0.4^m/arcsec^2 for SB0 galaxies and 1.5 ± 0.4^m/arcsec^2 for SB0/Ba–SBbc galaxies to 2.3 ± 0.4^m/arcsec^2 for SBc–IBm galaxies; i.e., bars in late-type galaxies are photometrically more distinct against the disk background than those in early-type galaxies.

3.2. Integrated Bar Color Indices

The average color indices of the bars are essentially independent of the morphological type of the parent galaxy. The only exceptions are the color indices $(B-V)_0$ and $(R-I)_0$ (Table 1). Estimates of U brightnesses and $(U-B)_0$ are too scarce for us to derive reliable average values. Late-type galaxies have appreciably lower $(B-V)_0$ and $(R-I)_0$ values than do SB0–SBbc galaxies. Precisely these low $(B-V)_0$ values are responsible for the relatively higher brightness of the bars in late-type galaxies at blue wavelengths.

The bars in all galaxies display the same infrared color indices; their average surface brightnesses, however, are different and depend on the morphological type of the galaxy (see the electronic table and Table 1). The infrared data for SB0 galaxies are untrustworthy due to their poor statistics.

The distribution of the $(B-V)_0$ color indices of the bars is of special interest. The corresponding histogram is presented in Fig. 2a, while, for comparison, Fig. 2b shows the distribution of the integrated $(B-V)_0$ values from the RC3 catalog. While the integrated color indices of the galaxies are well correlated with their morphological types (Fig. 2b), there is a pronounced peak in the bar distribution at $(B-V)_0 = 0.8^m$. The bars in SB0 and SB0/Ba–SBbc galaxies have essentially the same colors (Table 1); only in extremely late-type galaxies are the bars, on average, 0.2^m bluer. Thus, the influence of galactic morphological type on bar color is weaker than its influence on the average bar surface brightness.

We can interpret the data in Fig. 2a and Table 1 as follows. In the bars of late-type galaxies (SBc–IBm), star formation is more active and the contribution of the young stellar population to the total luminosity larger than in bars in early-type galaxies (SB0–SBbc). Therefore, $(B-V)_0$ and $(R-I)_0$, which are sensitive to star formation, are lower in the bars of late-type galaxies than in those of SB0–SBbc galaxies. The lack of such a dependence for $(U-B)_0$ is probably due to the poor statistics for bars in early-type galaxies (Table 1). This may also be related to the fact that the stellar populations in galaxies of different morphological types have different age distributions (a displacement from the normal color sequence for galaxies in the $(U-B)_0$–$(B-V)_0$ two-color diagram).

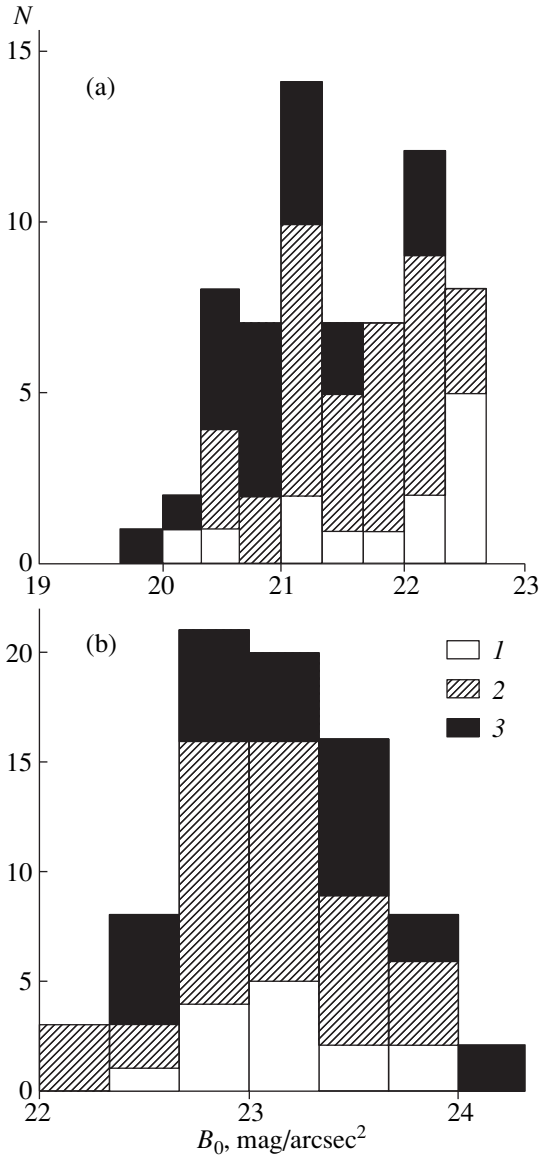

Fig. 1. Distributions of the number of galaxies as a function of (a) average bar surface brightness and (b) intrinsic average surface brightness. *1*—SB0 galaxies, *2*—SB0/Ba–SBbc galaxies, *3*—SBc–IBm galaxies.

3.3. Location of the Bars in Two-Color Diagrams

Of the 100 galaxies in our sample (see Section 2), 42 have data for two or more *UBVRI* color indices for their bars. We studied the locations of the bars in three two-color diagrams: $(U-B)_0$–$(B-V)_0$, $(B-V)_0$–$(V-R)_0$, and $(B-V)_0$–$(V-I)_0$ (Figs. 3a, 3b, and 3c, respectively). The straight line in the diagrams indicates the normal sequence for the integrated colors of galaxies (NCS), taken from the study of Buta and Williams [18], who used the color indices for 501 galaxies

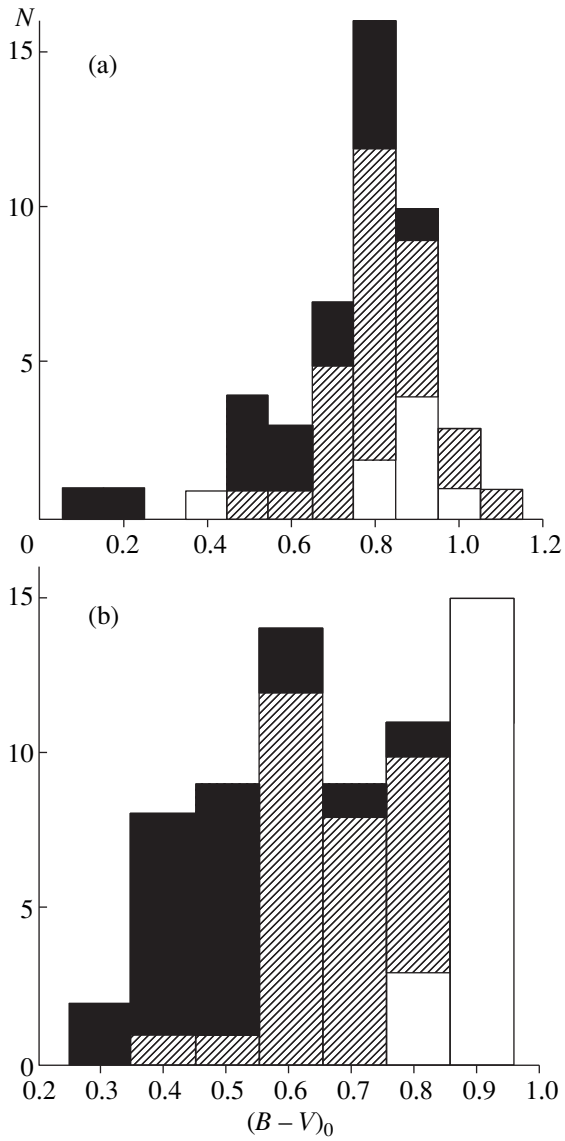

Fig. 2. Distributions of the number of galaxies as a function of (a) $(B-V)_0$ for their bars and (b) intrinsic $(B-V)_0$. The types of galaxies are denoted as in Fig. 1.

from the RC3 [16]. The sequences derived by Buta and Williams [18] are consistent with those obtained in previous studies, based on both observations and simulations of galaxy colors. For comparison, Fig. 4 presents two-color diagrams with the locations for the galaxies in our sample indicated (we used the integrated color indices from [16] and [18]).

As we can see in Fig. 3, most of the bars are located to the left of the NCS, most noticeably in the $(B-V)_0$–$(V-R)_0$ diagram. The $(U-B)_0$–$(B-V)_0$ two-color diagram is of special interest. Here, in most cases, only the bars of late-type galaxies, starting with type SBc, are located to the left of the NCS. However, the poor statistics for early-type galaxies with known $(U-B)_0$ values prevent us from determining whether the bars of early- and late-type galaxies diverge. In most cases, the errors in the brightnesses and colors of the bars in our sample are 0.1^m (see the electronic table). For a sample of bars in galaxies without an intense burst of star formation with more accurately determined color indices, the number of bars located to the right of the NCS in two-color diagrams (including $(U-B)_0$–$(B-V)_0$) becomes essentially zero (see, for example, Fig. 5a).

Galaxies of different morphological types are clearly separated in the two-color diagrams: late-type galaxies are located to the left of and above early-type galaxies (Fig. 4). The location of bars in the two-color diagrams depends on the parent galaxy type much more weakly (Fig. 3). This is consistent with the result described in Section 3.2: the color indices of bars depend only weakly on the morphological type of the parent galaxy.

The integrated color indices for a few of the late-type galaxies in our sample are displaced to the right of the NCS (Figs. 4b, 4c). This probably reflects the presence of starburst galaxies in the sample. At the same time, there are no appreciable differences in the positions of barred and unbarred galaxies in the two-color diagrams [18].

We will consider below a possible explanation for the displacement of the bar color indices to the left of the normal color sequence for galaxies.

3.4. Color Variations along the Bar Major Axis

In a number of studies (Table 2), variations of colors along bars as a function of distance from the center can be traced. The results are presented in Fig. 5. To reduce the number of figures, we present a $(U-V)_0$–$(V-R)_0$ diagram instead of the commonly used $(B-V)_0$–$(V-R)_0$ diagram (see Table 2). In total, ten galaxies were studied in this way. With only one exception (NGC 1620), we can clearly see a deviation of the bar color indices in the two-color diagram toward the left; i.e., the bars become bluer with increased distance from the galaxy nucleus.

The bars of all galaxies lie to the left of the NCS in the two-color diagrams. The two exceptions are the bars in the peculiar galaxy NGC 5665 and the starburst galaxy NGC 6217. The bars of these galaxies lie to the right of the NCS (Fig. 5; the opposite parts of the bars in NGC 5665 and NGC 6217 are displayed separately). This reflects the known fact that a burst of star formation in an old stellar system displaces the points in two-color diagrams toward the right [18].

3.5. A Possible Origin for the Anomalous Color Indices of Bars

An anomalously low bar $(V-R)_0$ color index compared to the integrated disk color was first noted in the $(B-V)_0$–$(V-R)_0$ two-color diagram for the galaxy NGC 4027 by Pence and de Vaucouleurs [24]. They explained the displacement of the integrated bar color-

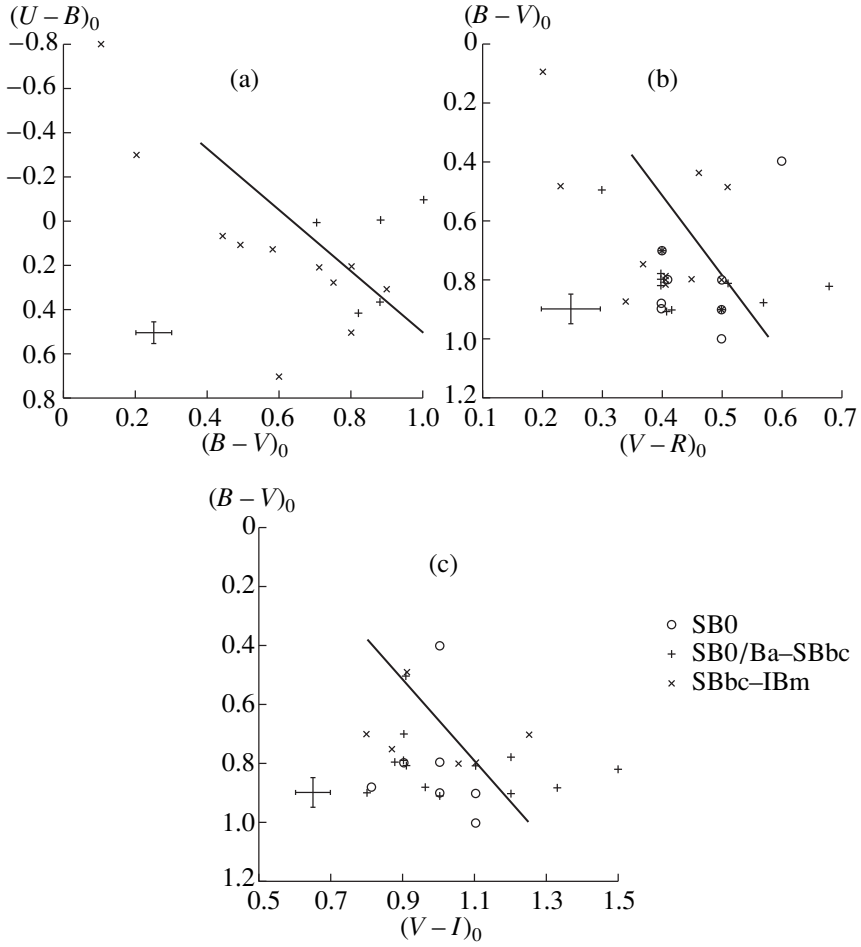

Fig. 3. (a) $(U-B)_0$–$(B-V)_0$, (b) $(B-V)_0$–$(V-R)_0$, and (c) $(B-V)_0$–$(V-I)_0$ two-color diagrams for the bars. The different symbols denote galaxies of different morphological types. The straight lines represent the NCS of galaxies. The observational errors for the bar color indices are indicated.

index points to the left of the NCS as a consequence of the relatively low H_α flux from the area occupied by the bar. However, this is not a plausible explanation for the displacement of the bar color indices in the $(U-B)_0$–$(B-V)_0$ diagram.

Odewahn [4] also detected a displacement of the color indices of the bar of NGC 4618 to the left of the NCS in $(B-V)_0$–$(V-I)_0$ and $(B-V)_0$–$(B-I)_0$ diagrams. He explains the anomalously blue $(V-I)_0$ of the bar relative to the integrated disk colors as the effect of enhanced formation of massive stars in the bar. The initial mass function (IMF) of stars can, indeed, differ from the classical function in the regions of intense shock waves observed in bars: in these areas, relatively large numbers of massive stars can form. However, the excess of massive, young stars should have an even greater effect on the bar's $(B-V)_0$, which is not seen for NGC 4618, whose bar and disk have the same $(B-V)_0$.

Using the $(U-B)_0$–$(B-V)_0$ diagram, Esipov *et al.* [11] considered variations in the color indices of the bar of NGC 151 along the bar's major axis as a function of distance from the center. They attribute the bluer color of the outer areas of the bar to an increase in the contribution of young stars (with ages less than 10^9 yrs) at the peripheral zones of the bar. At the same time, they suggest that the displacement of the bar color-index points to the left of the NCS reflects a scarcity of intermediate-age stars (~10^9 yrs) in the bar. This situation can arise if stars formed in the bar leave it shortly thereafter.

The displacement of the color indices of a stellar system to the right or left of the NCS in two-color diagrams can, indeed, be explained by an absence of intermediate-age stars in the system (or an excess of both old and young stars at the same time); the presence of stars with ages of the order of 10^9 yrs, with no old and young stars; or an IMF such that a relative excess of massive stars is formed. Model calculations for the color indices of such stellar systems have not been carried out previously.

Neither the presence of dust nor the occurrence of a burst of star formation in a stellar system can displace a galaxy's color indices to the left of the NCS in two-

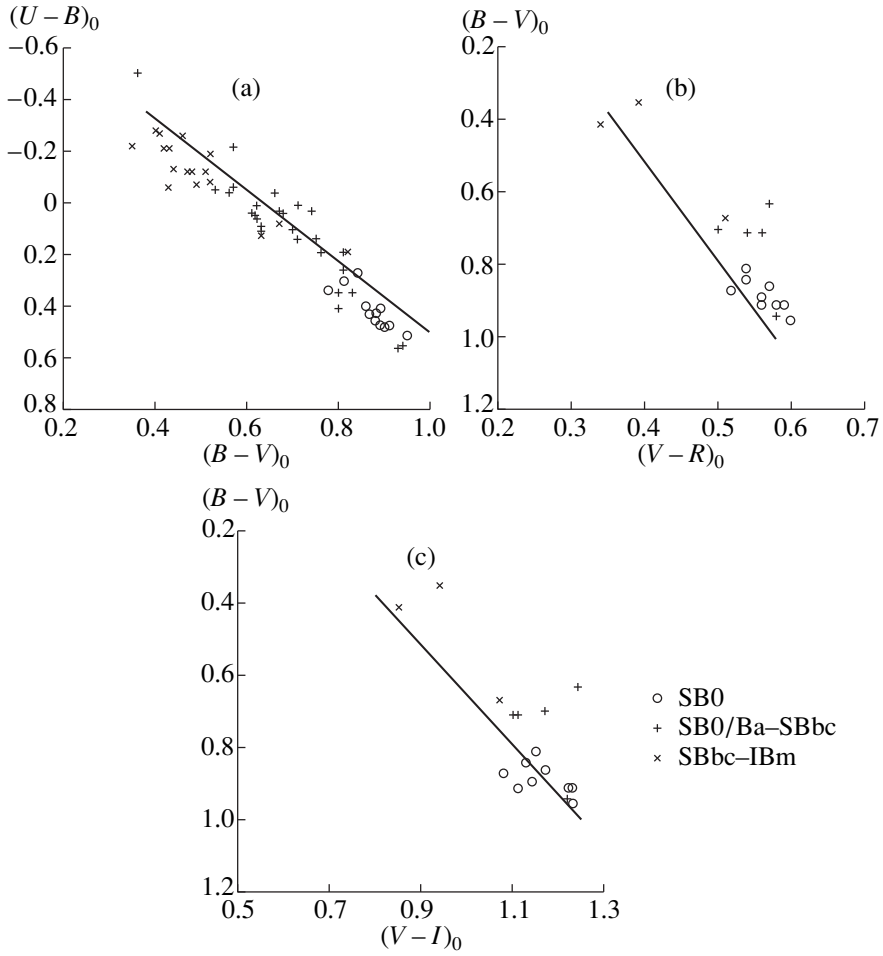

Fig. 4. (a) $(U-B)_0$–$(B-V)_0$, (b) $(B-V)_0$–$(V-R)_0$, and (c) $(B-V)_0$–$(V-I)_0$ two-color diagrams for the integrated colors of barred galaxies. The different symbols denote galaxies of different morphological types. Smaller symbols denote galaxies from our sample that are not included in the list of Buta and Williams [18]. The straight lines represent the NCS of galaxies (according to [18]).

color diagrams. A burst of star formation will displace points toward the right; stable, intense star formation (for example, with a constant star-formation rate) will displace them upward and to the left along the NCS [25]; the presence of strong absorption will shift them downward and to the right along the NCS [18]. Systems with stellar populations indicating an increased heavy-element abundance deviate from the NCS only in the $(U-B)_0-(B-V)_0$ diagram (in other diagrams, the displacement is along the NCS). Therefore, in our modeling of the population in a stellar system, we considered only the three cases mentioned above: (a) a deficit of intermediate age stars, (b) the presence only of intermediate age stars, and (c) an excess of massive stars.

4. MODELING THE STELLAR POPULATIONS OF GALACTIC BARS

4.1. Method and Initial Parameters

We used an evolution modeling technique to investigate the stellar populations of galactic bars. We adopted the PEGASE code developed in the Paris Institute for Astrophysics by M. Fioc and B. Rocca-Volmerange [26] and also the code developed by G. Worthey [27]. In the simulation with the PEGASE code, we used the Padua stellar library of evolutionary tracks for stars with $Z = 0.02$ [28]. The IMF suggested by Kennicutt [29] was adopted, which, in our opinion, is best suited to studies of the stellar populations of galaxies (see, for example, the discussion on different IMFs in [30]). In the modeling with Worthey's code [27], we used the Lick stellar library of evolutionary tracks and a Salpeter IMF.

One important feature of our modeling of the color indices of stellar systems is that, unlike the models acquired with the PEGASE code [26], Worthey's code [27] takes into account the evolution of the chemical composition of the system. We took the $Z(t)$ dependence for galaxies of various morphological types from the results obtained using the PEGASE code. When, in the course of evolution of the stellar system, the value $Z = 0.02$ was reached at some time t_Z, it was assumed that the stars formed from that point on possess solar chemical composition.

Table 2. Color variations along the bar major axis

NGC	Type	Two-color diagrams	References	Notes
151	SBbc	$(U-B)_0$–$(B-V)_0$	[8]	–
523	pec	$(U-B)_0$–$(B-V)_0$	[19]	–
1620	SBc	$(U-B)_0$–$(B-V)_0$	[20]	–
5605	SABcp	$(B-V)_0$–$(V-R)_0$ $(B-V)_0$–$(V-I)_0$	[21]	–
5665	SABcp	$(B-V)_0$–$(V-R)_0$ $(B-V)_0$–$(V-I)_0$	[21]	Northwestern and southeastern parts of the bar were considered separately
6217	SBbc	$(U-B)_0$–$(B-V)_0$ $(B-V)_0$–$(V-R)_0$ $(B-V)_0$–$(V-I)_0$	[22]	Northern and southern parts of the bar were considered separately
7292	Irr	$(U-V)_0$–$(V-R)_0$	[20]	–
7479	SBc	$(U-B)_0$–$(B-V)_0$	[23]	–
7678	SABc	$(U-B)_0$–$(B-V)_0$	[19]	–
7743	SB0/Ba	$(U-B)_0$–$(B-R)_0$	[20]	The bar $(B-V)_0$ values obtained in [18] were used to represent the galaxies in Figs. 5b and 5c

Unfortunately, when using the Lick stellar library of evolutionary tracks, Worthey's code [27] enables modeling only of old stellar systems (with ages of the stars $\geq 1 \times 10^9$ yrs). To take into account the contribution of young stars (with ages less than 1×10^9 yrs), we used the PEGASE code [26] with a Salpeter IMF.

The age of the galaxies T was taken to be 1.2×10^{10} yrs. The parameter describing the time dependence of the star-formation rate (SFR) was a variable. Let us consider this dependence in more detail. Sandage [31] proposed simple empirical laws to describe the time dependence of the SFRs for galaxies of various types. In elliptical galaxies, the SFR decreases exponentially as a function of time (on a shorter time scale than in spiral galaxies); in S0–Sc galaxies, the SFR is, in general, proportional to the mass of the gas in the galaxy at that time (i.e., the star-formation efficiency is constant with time, while the SFR decreases exponentially); in Sd galaxies, the SFR is constant. Following Sandage, we used these three time dependences for the SFRs.

Corresponding formulas are presented in Table 3; M is the total mass of the galactic disk. We took the time dependence of the SFR for elliptical galaxies from [32]; the analogous dependences for spiral galaxies were chosen based on standard SFRs and star-formation efficiencies for early- and late-type galaxies derived from observations. For brevity, we will call the SFR time dependences in Table 3 "normal."

In modeling stellar systems without intermediate-age stars (we denote the ends of the age interval $t_{\min}$ and $t_{\max}$), we used the following procedure to tie the NCS obtained from color-index simulations to the NCS derived observationally (in the diagrams, the model and observed NCSs coincide to within 0.1^m). Initially, the *UBVRI* luminosities for systems with normal SFR time dependences were determined. Then, the data were tied to the NCS used in Section 3.3 (adopting the values for L_B and $(B-V)_0$ as "zero points"). Further, we determined the *UBVRI* luminosities for a system with no star formation from 1.2×10^{10} yrs ago to $t_{\max}$ and from $t_{\min}$ to the present time, and with the normal SFR time dependence during the time from $t_{\max}$ to $t_{\min}$ (the input parameters were normalized accordingly). Finally, the *UBVRI* luminosities obtained in the first and second cases were subtracted. In this way, we obtained luminosities in these bands for systems with no stars with ages from $t_{\min}$ to $t_{\max}$. In total, we considered 11 models for each of the three types of galaxies: nine models using the PEGASE code [26] (systems without stars with ages 0.5–1, 0.5–3, 0.5–5, 0.5–9, 1–3, 1–5, 1–9, 3–5, and $(5–9) \times 10^9$ yrs) and two using Worthey's code [27] (systems with no stars with ages 1–9 and $(1–11) \times 10^9$ yrs).

We modeled stellar systems populated exclusively by intermediate-age stars using the PEGASE code. We assumed that, over some time interval, all the matter in the system would be converted to stars at some constant SFR. We considered five models: systems in which all stars are formed during intervals of 10^6, 10^7, 10^8, 10^9, and 3×10^9 yrs.

When modeling stellar systems with an excess of massive stars, we used the PEGASE code and varied the IMF. We considered the following two cases.

(1) The IMF corresponds to Kennicutt's [29] IMF for stars with masses $0.1–1 M_\odot$ ($f(M) \sim M^{-1.4}$) and differs from it for stars with masses $1–120 M_\odot$ ($f(M) \sim M^{-2.5}$ is the standard Kennicutt IMF [29], and we used $f(M) \sim M^{-\alpha}$ for the models). We considered six models for each of

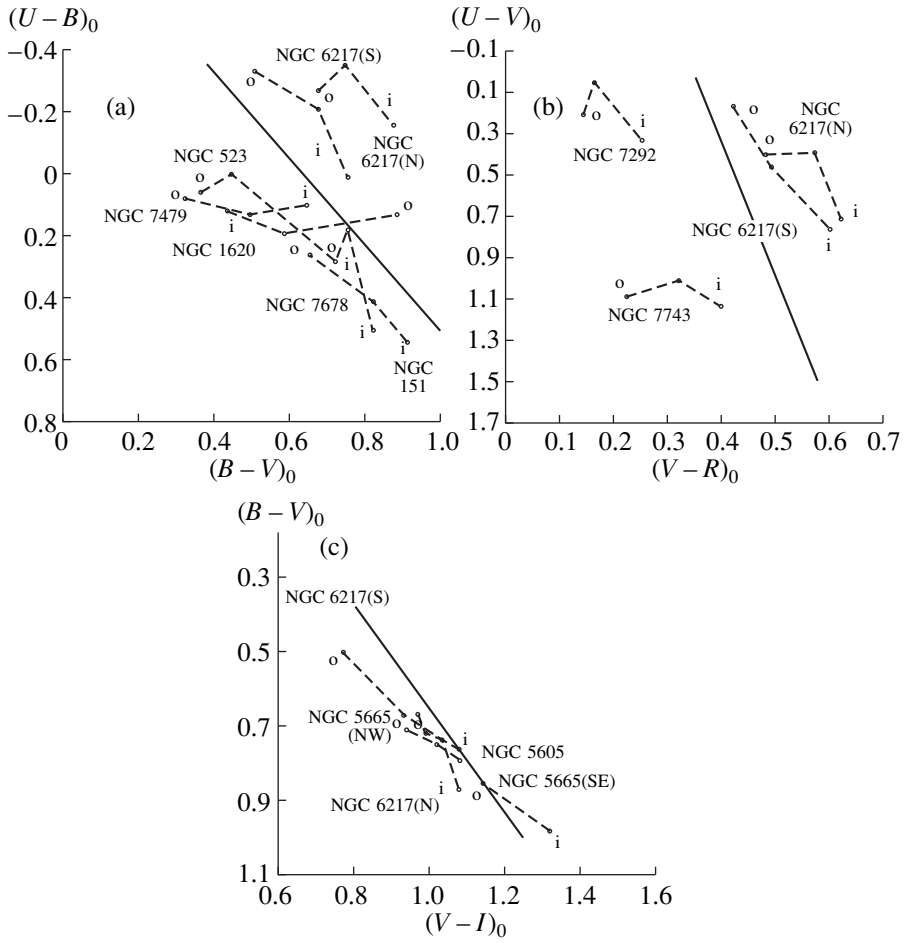

Fig. 5. (a) $(U-B)_0$–$(B-V)_0$, (b) $(U-V)_0$–$(V-R)_0$, and (c) $(B-V)_0$–$(V-I)_0$ two-color diagrams. The dashed curves show variations in the color indices along the bar semimajor axis from inner ("i") to outer ("o") areas. The solid lines show the NCS of galaxies.

the three types of galaxies: systems with IMFs for stars with masses 1–120$M_\odot$ with indices α = 2.2, 2.0, 1.8, 1.6, 1.4, and 1.2.

(2) The IMF of the system corresponds to Kennicutt's [29] IMF for stars with masses larger than some M_{crit} and is zero for stars with lower masses. We considered three models for each of the three types of galaxies: systems with M_{crit} = 1, 3, and 10$M_\odot$.

4.2. Model Results

Figures 6 and 7 present two-color diagrams with color sequences for the systems without intermediate-age stars. The systems with SFRs corresponding to those of late-type galaxies are in the upper left corners of the diagrams, while those with SFRs corresponding to those of elliptical galaxies are in the lower right corners. With the exception of the active starburst galaxies (see Sections 3.3, 3.4), the observed bar color indices are also plotted in these diagrams. Note that most of the model sequences deviate from the NCS by only a very small amount, only slightly exceeding the error intervals for the color indices of most bars. However, the accuracy of the color indices for the bars in the galaxies in Table 2 is sufficient for meaningful comparisons with the model dependences.

Table 3. SFRs for galaxies of different morphological type

Galaxies	SFR
Ellipticals	$1.2\times10^{-9}M\exp(-t/10^9)$
Early-type spirals	$5\times10^{10}M\exp(-t/3.1\times10^9)$
Late-type spirals	$10^{-10}M$

The model color sequences for stellar systems without stars with ages (1–9) $\times 10^9$ yrs acquired using the PEGASE [26] and Worthey [27] codes are somewhat different (cf. Figs. 6 and 7). The largest discrepancy can be seen for the model colors of early-type galaxies. This is largely due to the different chemical compositions of the old stellar populations in the model systems obtained using the two codes. The contribution of the old stellar population to the total luminosity of a system decreases from early- to late-type galaxies (see below). For this reason, in the two-color diagrams, the positions

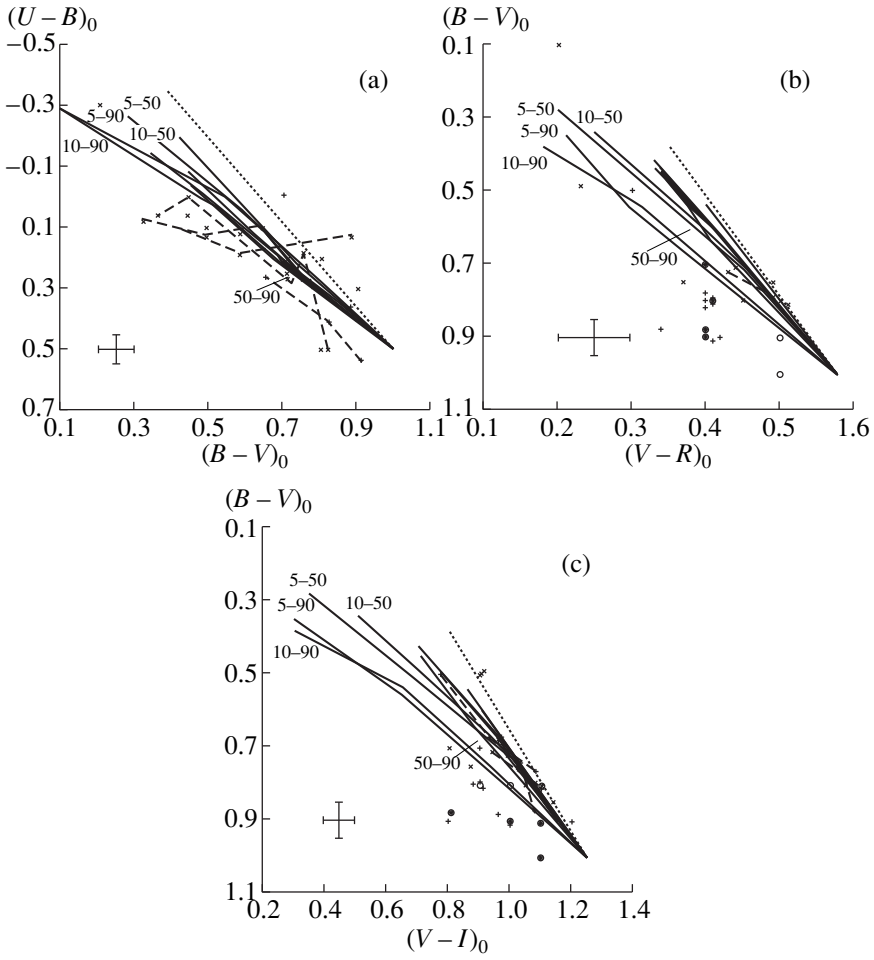

Fig. 6. Model sequences (solid) for systems without intermediate-age stars (age intervals in 10^8 yrs are denoted by the numbers) in the (a) $(U-B)_0$–$(B-V)_0$, (b) $(B-V)_0$–$(V-R)_0$, and (c) $(B-V)_0$–$(V-I)_0$ two-color diagrams, obtained using the PEGASE code. Systems with SFRs corresponding to late-type galaxies are located in the upper left corner, while systems with SFRs corresponding to elliptical galaxies are in the lower right corner. The dotted lines represent the NCS of galaxies. For comparison, the dashed lines indicate the observational data for bars in galaxies that are not undergoing active bursts of star formation (the labels are the same as in Fig. 5). The observational errors for the bar color indices are indicated.

of systems with SFRs corresponding to those typical of late-type galaxies obtained using the PEGASE [26] and Worthey [27] codes differ only slightly (Figs. 6, 7).

As we can see from Figs. 6 and 7, the color indices for models without intermediate-age stars are displaced in the same direction from the NCS as the observed color indices of most bars. Most bars in galaxies with low SFRs occupy the area in the two-color diagrams corresponding to stellar systems without stars with ages $(1–9) \times 10^9$ yrs (Figs. 6, 7).

In the $(U-B)_0 - (B-V)_0$ diagram, points corresponding to the outer parts of the bars of most galaxies lie to the left of the model color sequences. It is likely that the OB associations located at the ends of these bars are so intense that they totally dominate the radiation from the old stellar population in the outer areas of the bars (for systems without star formation $(1–9) \times 10^9$ yrs ago, the fraction of stars younger than 10^9 yrs making up the total B luminosity varies from 94% for late-type galaxies and 77% for early-type galaxies to 0.07% for elliptical galaxies).

The slight deviation of the bars from the model sequences in the $(B-V)_0 - (V-R)_0$ and $(B-V)_0 - (V-I)_0$ diagrams may be due to selective absorption: the bars have a rather large amount of dust (see Section 1). The $(U-B)_0 - (B-V)_0$ diagram is less sensitive to internal absorption in stellar systems, since the model sequences here deviate from the NCS to a smaller degree.

On the whole, the model color sequences for systems without intermediate-age stars in all the two-color diagrams can account for the positions of most of the observed bars. The model color sequences for systems without stars with ages $(0.5–9) \times 10^9$, $(1–9) \times 10^9$, and $(1–11) \times 10^9$ yrs in the $(B-V)_0$–$(V-R)_0$ and $(B-V)_0$–$(V-I)_0$ diagrams virtually coincide. This prevents us from more accurately determining the age interval for the stars that are deficient in the bars.

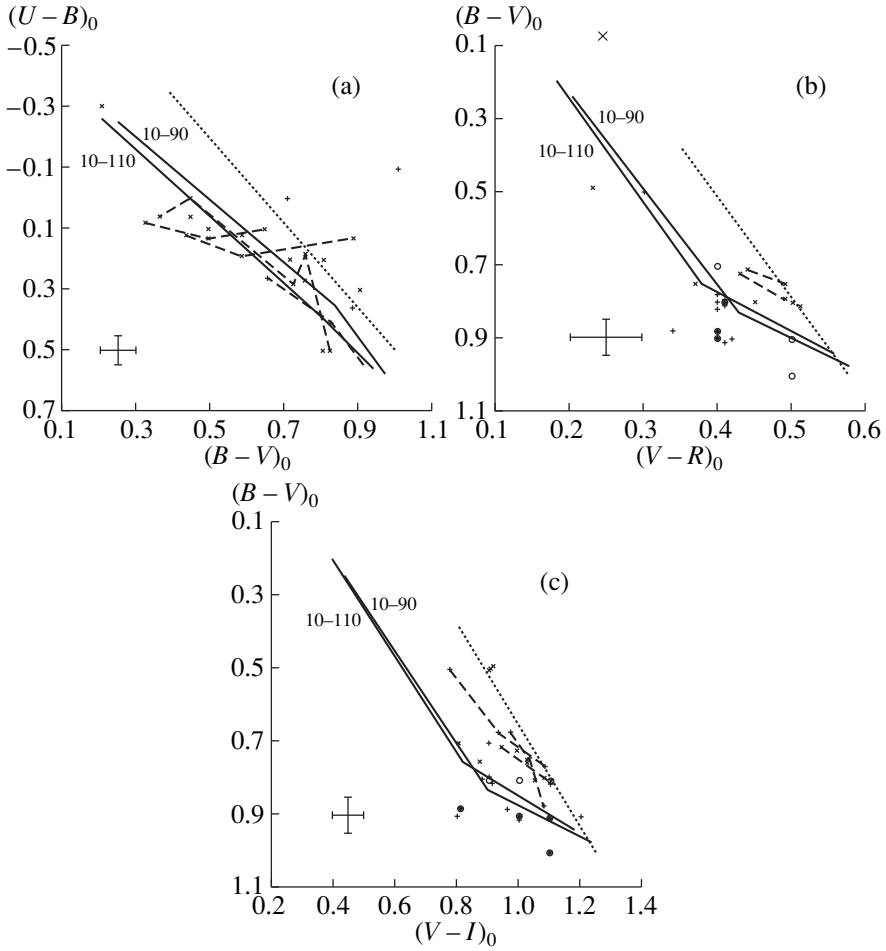

Fig. 7. Same as Fig. 6 for the model sequences obtained using Worthey's [27] code.

Our modeling for the color indices of stellar systems with nonstandard initial mass functions and systems with only intermediate-age stellar populations showed inconsistency between the model sequences and observed bar color indices. As an example, the two-color diagrams in Fig. 8 show evolutionary tracks for systems with stellar populations of approximately the same age. In the $(U-B)_0$–$(B-V)_0$ diagram, most galactic bars do indeed have the same colors as stellar systems consisting only of stars with intermediate ages (5×10^8–3×10^9 yrs). However, in the $(B-V)_0$–$(V-R)_0$ and $(B-V)_0$–$(V-I)_0$ diagrams, most bars are located far to the side of the evolutionary tracks. The model sequences for systems with nonstandard IMFs (systems without low-mass stars or those with a more sloping IMF) are also located either along or to the right of NCS, so that they are even less consistent with the observations for the bars.

Therefore, the displacement of the bar color indices to the left of the NCS is most likely due to a deficit of intermediate-age stars. The fact that there is a relative deficit of star clusters with ages 5×10^8–6×10^9 yrs in the bar of the Large Magellanic Cloud [33] supports this conclusion.

5. DISCUSSION

The deficit of intermediate-age stars in bars can be understood as a result of the fact that, after the formation of the bar, the stars formed in it leave the bar within about 10^9 yrs [11]. The hypothesis that a relatively young bar (formed later than 10^9 yrs ago) is observed against the background of an older disk stellar population is not suitable here, since, for the standard SFR, we would observe for all types of spiral galaxies (including SB0) only an excess of young stars against the background of the standard stellar population.

Bars in early-type galaxies form over periods of 2×10^8–1.2×10^9 yrs [34, 35]. From the time of its formation, the bar potential has a profound impact on the dynamics of the stars and gas in the galaxy. Old stars in the bar move along very elliptical orbits (the x_1 set of orbits, according to the nomenclature of [13]). Radial movements of gas along the bar can result in the formation of an active nucleus in early-type galaxies and in a burst of star formation in late-type galaxies [36, 37]; at the same time, radial gas movements can increase the gas density at the ends of the bar and, consequently,

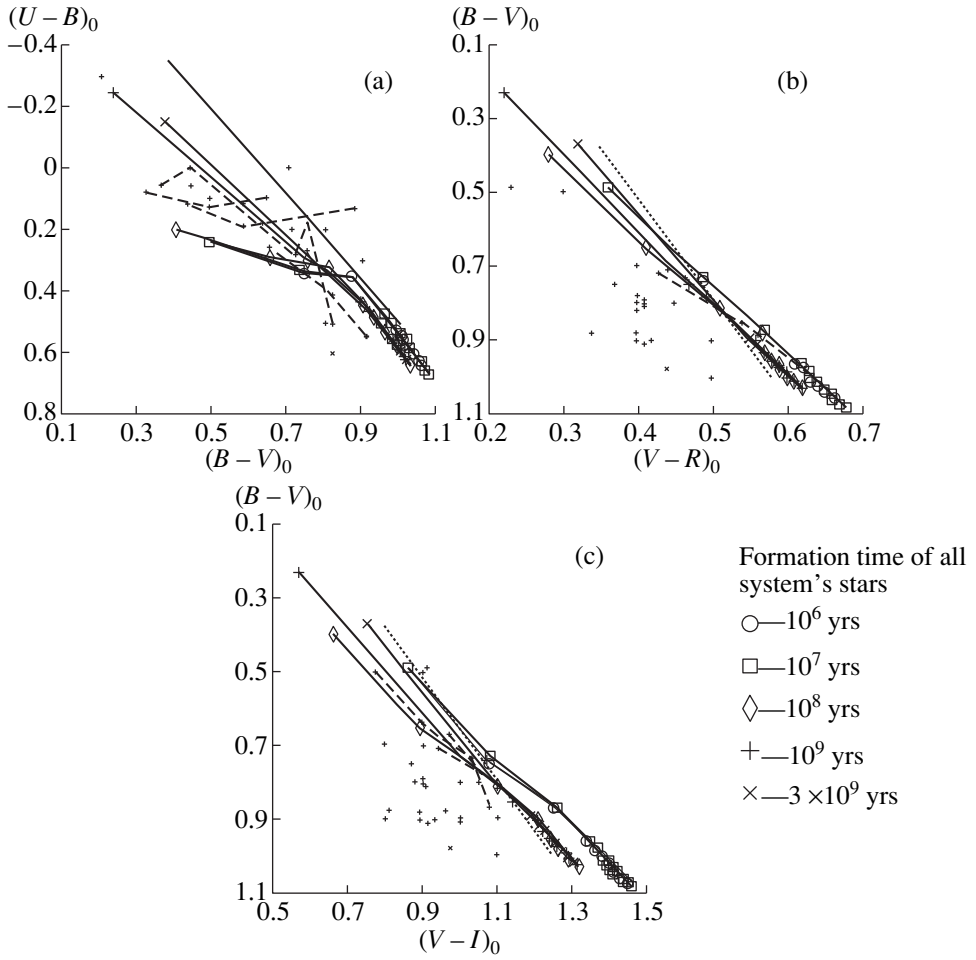

Fig. 8. (a) $(U-B)_0$–$(B-V)_0$, (b) $(B-V)_0$–$(V-R)_0$, and (c) $(B-V)_0$–$(V-I)_0$ two-color diagrams with evolutionary tracks for stellar systems (solid curves) with bursts of star formation that lasted for some time, after which star formation ceased. The corresponding symbols indicate the locations of systems with ages of 0.5, 1, 2, 3, …, 12×10^9 yrs whose stars were formed within 10^6, 10^7, or 10^8 yrs; of systems with ages of 1, 2, 3, …, 12×10^9 yrs whose stars were formed within 10^9 yrs; and of systems with ages of 3, 4, 5, …, 12×10^9 yrs whose stars were formed within 3×10^9 yrs. Time is measured from the start of the burst of star formation 1.2×10^{10} yrs ago. The systems evolve from the upper left corner to the lower right corner of the diagrams. The dotted line represents the NCS of galaxies. The asterisks correspond to the observed color indices of bars in galaxies that are not undergoing active bursts of star formation.

intensify the star formation there [38]. In the presence of inner Lindblad resonance, gas clouds reach the bar at some angle (at an angle of 90° for two inner Lindblad resonances), forming a shock wave at the leading edge of the bar [39]. Before passing through the shock, the gas has a low density and, in the general case, moves toward the end of the bar. After its passage through the shock, the now high-density gas moves toward the nucleus of the galaxy. Dust lanes are an observational manifestation of this shock; appreciable star formation is not observed along these lanes in the bars of early-type galaxies [38].

Thus, in bars that do not contain a large amount of gas, stars form primarily near the nucleus and in the outer regions of the bar [40]. The stars that form move in either circular orbits about the nucleus or in highly elliptical orbits about the bar major axis (the orbits for old bar stars are less elliptical). However, in the regions of the bar that are most distant from the center, radial stellar orbits become unstable, since they end up either in the region of inner Lindblad resonance (the outer boundary of bars in late-type galaxies) or at a distance corresponding to the corotation radius (the inner boundary of bars in early-type galaxies). In addition, the bar potential is capable of dynamically heating the disk due to the presence of both vertical and horizontal inner Lindblad resonances: stars forming in the disk and bar can leave the galactic plane, enriching the bulge [35, 37, 41].

This picture is valid for bars that have formed due to the instability of a rapidly rotating disk. No serious gas and stellar dynamics studies have been carried out for galaxies with bars whose formation is due to instability of radial orbits (the Lynden-Bell mechanism). It is likely, however, that the stellar and gas dynamics in

bars of this type are similar to those described above. This conclusion is supported by the fact that two-color diagrams do not show any significant differences in the locations of bars belonging to galaxies of different morphological types (see Section 3.3) and also by the detection of dust lanes in the bars of galaxies of all morphological types ranging from SB0 to SBm. The only differences between bars of late- and early-type galaxies are that the former have an exponential brightness decrease along the bar major axis [2] and that the star formation in these bars occurs along the entire length of the bar [37]. The formation time for such bars (~10^8 yrs [15]) roughly corresponds to that for bars in rapidly rotating disks. The influence of the bar on the motions of stars and gas in the bar region is probably the same, independent of how the bar was formed.

Thus, young and old stars in the bar have different trajectories of motion. It seems likely that young stars formed at the ends of the bar gradually leave it and enter the inner areas of the disk and bulge. However, the supply of gas to the bar, and consequently the star formation in it, must be continuous, since young stars (younger than 5×10^8–1×10^9 yrs) are observed in bars. Star formation is most intense at the ends of bars, since a large amount of gas is concentrated there, so that the stellar population becomes younger as we approach the ends of bars. Older stars that appeared before and at the time of formation of the bar are also always present in bars.

Another possible explanation for the deficit of intermediate-age stars in bars is the ejection of stars from outer areas of the bar into the inner circumnuclear area of the bar. In this case, the radiation of these stars will be suppressed by that from the nucleus and bulge of the galaxy.

The aperture photometry data presented in Table 2 indicate that, in apertures with diameters equal to, or slightly larger than, the length of the bar, the $(U-B)_0$, $(B-V)_0$, and $(V-R)_0$ values correspond to the NCS; i.e., the stars in galaxies at distances not exceeding the bar semimajor axis are consistent with a standard population. This is possible only if intermediate-age stars leave the bar and supplement the stellar population of the inner part of the disk (or the circumnuclear region).

We thus conclude that the deficit of intermediate-age stars in galactic bars is due to the fact that stars that form in the bar leave it within a few rotations. This may be due to the different trajectories displayed by young and old stars in the bar. The motion of stars in the gravitational potential of a bar will be considered in more detail in a future study.

6. CONCLUSIONS

(1) The distribution of the average surface brightnesses of galactic bars displays two peaks: the first ($B_0 = 21.0^m$/arcsec^2) is characteristic of bars of late-type galaxies and the second ($B_0 = 22.2^m$/arcsec^2) of bars of early-type galaxies. Bars of both types occur in SB0/Ba–SBbc galaxies.

(2) The difference between the average surface brightnesses of the bar and of the galaxy as a whole increases from 1.1^m/arcsec^2 for SB0 galaxies to 2.3^m/arcsec^2 for late-type galaxies.

(3) We have confirmed the previously noted displacement of the color indices of bars in two-color diagrams to the left of the normal color sequence for galaxies.

(4) Bars become bluer with distance from the center: the corresponding points are displaced to the left and upward in two-color diagrams.

(5) The color indices of bars in galaxies of all morphological types suggest that the contribution of intermediate-age [$(1–9) \times 10^9$ yrs] stars is relatively small.

ACKNOWLEDGMENTS

I am grateful to A.V. Zasov and O.K. Sil'chenko of the Sternberg Astronomical Institute and V.P. Reshetnikov of St. Petersburg University for useful comments that substantially improved the manuscript. I thank O.Yu. Malkov, L.A. Sat, D.A. Kovaleva, and their colleagues from the Astronomical Data Center of the Institute of Astronomy of the Russian Academy of Science for access to the Center's electronic database. This study was supported by the Russian Foundation for Basic Research (project code 98-02-17102) and the State Science and Technology Program "Astronomy. Basic Research" (project 1.2.4.3).

REFERENCES

1. A. T. Kalloglian, Soobshch. Byurak. Obs., Akad. Nauk Arm. SSR **33**, 19 (1963).
2. B. G. Elmegreen and D. M. Elmegreen, Astrophys. J. **288**, 438 (1985).
3. D. M. Elmegreen, B. G. Elmegreen, F. R. Chromey, *et al.*, Astron. J. **111**, 1880 (1996).
4. S. C. Odewahn, Astron. J. **101**, 829 (1991).
5. M. W. Regan and D. M. Elmegreen, Astron. J. **114**, 965 (1997).
6. G. F. Benedict, J. L. Higdon, E. V. Tollestrup, *et al.*, Astron. J. **103**, 757 (1992).
7. A. T. Kalloglian, Soobshch. Byurak. Obs., Akad. Nauk Arm. SSR **25**, 35 (1958).
8. A. C. Phillips, Bull. Am. Astron. Soc. **25**, 1329 (1993).
9. I. I. Pronik, Izv. Krym. Astrofiz. Obs. **45**, 162 (1972).
10. B. G. Elmegreen, D. M. Elmegreen, F. R. Chromey, *et al.*, Astron. J. **111**, 2233 (1996).
11. V. F. Esipov, A. V. Zasov, and G. V. Popravko, Astron. Zh. **70**, 1 (1993) [Astron. Rep. **37**, 1 (1993)].
12. G. Contopoulos, Astron. Astrophys. **81**, 198 (1980).
13. G. Contopoulos and P. Grosbol, Astron. Astrophys. Rev. **1** (3/4), 261 (1989).
14. D. Lynden-Bell, Mon. Not. R. Astron. Soc. **187**, 101 (1979).

15. V. L. Polyachenko and E. V. Polyachenko, Pis'ma Astron. Zh. **20**, 491 (1994) [Astron. Lett. **20**, 416 (1994)].
16. G. de Vaucouleurs, A. de Vaucouleurs, H. G. Corwin, *et al.*, *Third Reference Catalogue of Bright Galaxies* (Springer Verlag, New York, 1991).
17. J. H. Elias, J. A. Frogel, K. Matthews, and G. Neugebauer, Astron. J. **87**, 1029 (1982).
18. R. Buta and K. L. Williams, Astron. J. **109**, 543 (1995).
19. B. P. Artamonov, V. V. Bruevich, and A. S. Gusev, Astron. Zh. **74**, 654 (1997) [Astron. Rep. **41**, 577 (1997)].
20. A. S. Gusev and V. F. Esipov, Astron. Zh. **73**, 357 (1996) [Astron. Rep. **40**, 319 (1996)].
21. B. P. Artamonov, Yu. Yu. Badan, and A. S. Gusev, Astron. Zh. (2000) (in press) [Astron. Rep. (2000) (in press)].
22. B. P. Artamonov, Yu. Yu. Badan, V. V. Bruevich, and A. S. Gusev, Astron. Zh. **76**, 438 (1999) [Astron. Rep. **43**, 377 (1999)].
23. G. F. Benedict, Astron. J. **87**, 76 (1982).
24. W. D. Pence and G. de Vaucouleurs, Astrophys. J. **298**, 560 (1985).
25. R. B. Larson and B. M. Tinsley, Astrophys. J. **219**, 46 (1978).
26. M. Fioc and B. Rocca-Volmerange, Astron. Astrophys. **326**, 950 (1997).
27. G. Worthey, Astrophys. J., Suppl. Ser. **95**, 107 (1994).
28. A. Bressan, F. Fagotto, G. Bertelli, and C. Chiosi, Astron. Astrophys., Suppl. Ser. **100**, 647 (1993).
29. R. C. Kennicutt, Jr., Astrophys. J. **272**, 54 (1983).
30. R. C. Kennicutt, Jr., P. Tamblyn, and C. W. Congdon, Astrophys. J. **435**, 22 (1994).
31. A. Sandage, Astron. Astrophys. **161**, 89 (1986).
32. Ch. Einsel, F.-V. Alvensleben, H. Kruger, and K. J. Fricke, Astron. Astrophys. **296**, 347 (1995).
33. A. S. Gusev, Astron. Zh. **75**, 506 (1998) [Astron. Rep. **42**, 446 (1998)].
34. F. Combes and B. G. Elmegreen, Astron. Astrophys. **271**, 391 (1993).
35. D. Friedli and L. Martinet, Astron. Astrophys. **277**, 27 (1993).
36. R. Arsenault, Astron. Astrophys. **217**, 66 (1989).
37. D. Friedli and W. Benz, Astron. Astrophys. **301**, 649 (1995).
38. E. Athanassoula, Mon. Not. R. Astron. Soc. **259**, 345 (1992).
39. F. Combes, in *The Formation and Evolution of Galaxies*, Ed. by C. Munoz-Tunon and F. Sanchez (Cambridge Univ., Cambridge, 1994), p. 317.
40. D. Reynaud and D. Downes, Astron. Astrophys. **337**, 671 (1998).
41. D. Pfenniger and C. Norman, Astrophys. J. **363**, 391 (1990).

Translated by K. Maslennikov